# Central Lancashire Online Knowledge (CLoK)

| Title | A rival for Babcock's star: the extreme 30-kG variable magnetic field in the Ap star HD 75049 |
|---|---|
| Type | Article |
| URL | https://clok.uclan.ac.uk/4619/ |
| DOI | https://doi.org/10.1111/j.1365-2966.2009.16015.x |
| Date | 2010 |
| Citation | Elkin, V. G., Mathys, G., Kurtz, D. W., Hubrig, S. and Freyhammer, L. M. (2010) A rival for Babcock's star: the extreme 30-kG variable magnetic field in the Ap star HD 75049. Monthly Notices of the Royal Astronomical Society, 402 (3). pp. 1883-1891. ISSN 00358711 |
| Creators | Elkin, V. G., Mathys, G., Kurtz, D. W., Hubrig, S. and Freyhammer, L. M. |

# A rival for Babcock's star: the extreme 30-kG variable magnetic field in the Ap star HD 75049[*]

V. G. Elkin,[1]† G. Mathys,[2] D. W. Kurtz,[1] S. Hubrig[3] and L. M. Freyhammer[1]

[1]*Jeremiah Horrocks Institute of Astrophysics, University of Central Lancashire, Preston PR1 2HE*
[2]*European Southern Observatory, Casilla 19001, Santiago 19, Chile*
[3]*Astrophysical Institute Potsdam, D-14482 Potsdam, Germany*

## ABSTRACT

The extraordinary magnetic Ap star HD 75049 has been studied with data obtained with the European Southern Observatory Very Large Telescope and 2.2-m telescopes. Direct measurements reveal that the magnetic field modulus at maximum reaches 30 kG. The star shows photometric, spectral and magnetic variability with a rotation period of 4.049 d. Variations of the mean longitudinal magnetic field can be described to first order by a centred dipole model with an inclination $i = 25°$, an obliquity $\beta = 60°$ and a polar field $B_p = 42$ kG. The combination of the longitudinal and surface magnetic field measurements implies a radius of $R = 1.7\,R_\odot$, suggesting that the star is close to the zero-age main sequence. HD 75049 displays moderate overabundances of Si, Ti, Cr, Fe and large overabundances of rare earth elements. This star has the second strongest magnetic field of any main-sequence star after Babcock's star, HD 215441, which it rivals.

**Key words:** stars: chemically peculiar – stars: individual: HD 75049 – stars: magnetic fields – stars: variables other.

## 1 INTRODUCTION

The complex processes of atomic diffusion – radiative levitation and gravitational settling – occur in upper main-sequence stars, and are particularly evident in chemically peculiar A-, B- and F-type stars, collectively known as Ap stars. Accordingly, these stars are good targets to place observational constraints on atomic diffusion, which is crucial for deepening our understanding of these processes within the framework of studies of the structure and evolution of stars, and for more global analysis of galactic chemical evolution. The Ap stars rotate considerably more slowly than spectroscopically normal main-sequence stars with similar effective temperatures. A fraction of Ap stars have extremely long rotation periods from tens of days to tens of years, and even of the order of a century in the case of $\gamma$ Equ. There is no clear picture of the braking mechanism leading to such slow rotation, but the observational evidence strongly suggests that it is related to the magnetic field (Mathys et al. 1997; Abt 2009).

Many Ap stars possess strong, predominantly dipolar magnetic fields. The first magnetic star, 78 Vir, was found by Babcock (1947). Eleven years later Babcock (1958) published the first catalogue of magnetic stars, and two years following that he discovered a huge 34 kG magnetic field in the star HD 215441 (Babcock 1960), known

since then as 'Babcock's star'. Despite success in the years that followed in increasing the number of known magnetic stars – especially in last several years (for example Hubrig et al. 2006; Kudryavtsev et al. 2006) – HD 215441 remains the record holder for the main-sequence star with the strongest magnetic field. The second strongest magnetic star, HD 154708, was discovered by Hubrig et al. (2005). Around the same time Kochukhov (2006) found HD 137509 to have magnetic field modulus of 29 kG. His result was in agreement with Mathys (1995) who discovered a very strong quadratic magnetic field of up to 37 kG in this star and mentioned that it has one of the strongest magnetic fields. Surprisingly, the longitudinal magnetic field in HD 137509 is not very large and varies just from $-1.25$ to $+2.35$ kG (Mathys 1991). HD 154708 still has the strongest magnetic field known among the cooler rapidly oscillating roAp stars (Kurtz et al. 2006).

The origin of the magnetic fields in Ap stars and details of their peculiar properties are still mysteries, despite large efforts in the study of these stars. As usual in physics, an analysis of extreme cases may provide key information, hence there is a great interest in the stars with the strongest magnetic fields to help solve many problems in Ap stars. Recently, Freyhammer et al. (2008) discovered an extremely strong magnetic field in Ap star HD 75049. Many lines in the high-resolution spectra are split into the clear Zeeman patterns. From the value of splitting, Freyhammer et al. (2008) estimated the photospheric magnetic field modulus to be about 30 kG. These observations also revealed a reasonably short rotation period, and large variability both of the magnetic field and the spectral line intensities. Because of these interesting characteristics of this rare

**Table 1.** A journal of high-resolution spectroscopic observations with UVES at the VLT and FEROS at the ESO 2.2-m telescope. The columns give the BJD of the middle of each exposure, the exposure time and the signal-to-noise ratio that was measured in sections of the continuum free of spectral lines.

| BJD | Exposure time (s) | S/N ratio | Instrument |
|---|---|---|---|
| 245 4141.669 63 | 1500 | 190 | FEROS |
| 245 4171.504 22 | 900 | 180 | UVES |
| 245 4387.815 93 | 1800 | 250 | UVES |
| 245 4432.824 89 | 1800 | 240 | UVES |
| 245 4451.833 66 | 1800 | 250 | UVES |
| 245 4455.702 26 | 1800 | 260 | UVES |
| 245 4468.845 89 | 1800 | 230 | UVES |
| 245 4481.814 65 | 1800 | 230 | UVES |
| 245 4513.788 92 | 1800 | 80 | UVES |
| 245 4516.689 04 | 1800 | 240 | UVES |
| 245 4524.664 61 | 1800 | 240 | UVES |
| 245 4544.516 08 | 1800 | 260 | UVES |
| 245 4547.511 27 | 1800 | 300 | UVES |
| 245 4557.590 95 | 1800 | 240 | UVES |

object, we have obtained a series of high-resolution spectra and carried out circular spectropolarimetric observations with the Very Large Telescope (VLT). We present in this paper the results of our analysis.

## 2 OBSERVATIONS AND DATA REDUCTION

To characterize the magnetic field of an Ap star, it is necessary to have magnetic measurements that cover the rotational phases of the star well. While we had a preliminary estimate for the rotation period of 4.05 d determined by Freyhammer et al. (2008) from All Sky Automatic Survey (ASAS) photometric survey data (Pojmanski 2002), we were uncertain about this, so we decided to spread new observations over half a year to be sure to determine the correct rotational period. There is also a possible 5.28-yr period in the ASAS data that was noted by Freyhammer et al. (2008). The nature of this long period is not clear, but it is certainly not a rotational period; the $v \sin i = 8.5 \, \mathrm{km \, s^{-1}}$ of HD 75049 does not allow that. Further understanding of this period will require long-term observations.

A series of high-resolution spectra was obtained in service mode using Ultraviolet and Visual Echelle Spectrograph (UVES) on the ESO VLT. 12 spectra were collected between 2007 October 10 and 2008 April 1. Two previous observations of this star with the Fiber-fed Extended Range Optical Spectrograph (FEROS) and UVES obtained in 2007 February and March were also used for this analysis. These observations were made with echelle spectrographs over long spectral regions. For FEROS, the spectral range is 3500–9220 Å with a resolution $R = \lambda/\Delta\lambda = 48\,000$; for UVES, the range is 4970–7010 Å with a resolution of $R = 110\,000$. A journal of these observations is presented in Table 1. Software packages provided by ESO (UVES and FEROS pipelines in the MIDAS environment) were used for the reduction and extraction of 1D spectra.

We also obtained spectropolarimetric observations of HD 75049 with the FOcal Reducer and low dispersion Spectrograph (FORS 1) in the VLT in service mode during the time-span 2007 December 30 to 2008 April 1. Observations with FORS 1 spectra in circular polarization are used for measurement of the longitudinal magnetic field, which corresponds to the line-of-sight component of the magnetic field vector integrated over the visible stellar hemisphere. This magnetic field parameter is sensitive to the magnetic field geometry and is very efficient for determining the rotational period.

Table 2 gives the Barycentric Julian Date (BJD) of the middle of each observation, the exposure time, phase of the rotational period and the results of the longitudinal magnetic field measurements for three different lists of spectral lines or spectral regions. A detailed description of similar spectropolarimetric observations and its reductions is given in the recent paper by Hubrig et al. (2009).

## 3 ROTATION PERIOD

The rotation period is an important parameter for the analysis of magnetic stars, which normally show photometric, spectral and magnetic variability with this period. In HD 75049, we found a clear picture of variability in all the three cases. As mentioned above, the photometric variability was detected in ASAS data, and spectral and magnetic variability were found from high-resolution spectra (Freyhammer et al. 2008). Our new longitudinal field measurements have allowed us to determine the rotation period with confidence and higher accuracy.

**Table 2.** Observations of HD 75049 with FORS 1. The columns give the BJD of the middle of each exposure, the rotational phase according to the ephemeris in equation (2) and the longitudinal magnetic field for two wavelength ranges of the spectrum and for the hydrogen lines with the error of measurement.

| BJD | Rotation phase | Longitudinal magnetic field $B_z$ (G) | | |
|---|---|---|---|---|
| | | 3212–6215 Å | 3705–6215 Å | Hydrogen lines |
| 245 4482.767 87 | 0.3978 | $-8894 \pm 68$ | $-8934 \pm 68$ | $-9744 \pm 132$ |
| 245 4483.609 47 | 0.6057 | $-9071 \pm 39$ | $-9096 \pm 39$ | $-9938 \pm 74$ |
| 245 4493.704 64 | 0.0989 | $-905 \pm 32$ | $-902 \pm 32$ | $-1475 \pm 61$ |
| 245 4516.733 63 | 0.7865 | $-4471 \pm 35$ | $-4485 \pm 35$ | $-5064 \pm 65$ |
| 245 4526.565 86 | 0.2148 | $-3538 \pm 40$ | $-3564 \pm 40$ | $-3970 \pm 74$ |
| 245 4527.581 59 | 0.4657 | $-9832 \pm 36$ | $-9857 \pm 36$ | $-10529 \pm 72$ |
| 245 4532.723 43 | 0.7356 | $-5811 \pm 49$ | $-5824 \pm 49$ | $-6367 \pm 91$ |
| 245 4539.771 71 | 0.4764 | $-9639 \pm 46$ | $-9661 \pm 46$ | $-10334 \pm 94$ |
| 245 4543.575 45 | 0.4158 | $-9237 \pm 39$ | $-9257 \pm 39$ | $-9941 \pm 75$ |
| 245 4546.521 95 | 0.1435 | $-1821 \pm 44$ | $-1818 \pm 44$ | $-2364 \pm 86$ |
| 245 4555.531 06 | 0.3685 | $-8139 \pm 33$ | $-8168 \pm 33$ | $-8528 \pm 64$ |
| 245 4557.619 44 | 0.8843 | $-1785 \pm 34$ | $-1793 \pm 34$ | $-2397 \pm 62$ |
| 245 4464.859 68 | 0.9749 | $-640 \pm 36$ | $-639 \pm 36$ | $-1415 \pm 68$ |
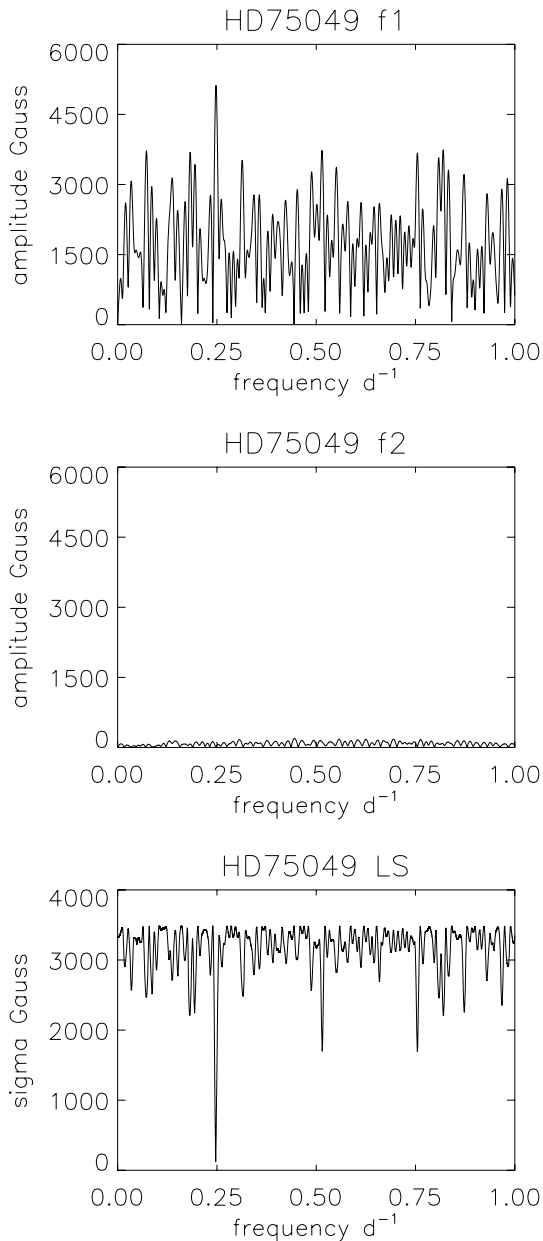
**Figure 1.** Frequency analysis of 13 FORS1 measurements of $B_z$ with times in BJD. The top panel shows the amplitude spectrum with the highest peak at $f = 0.2477 \, \text{d}^{-1}$. The middle panel shows the residuals on the same scale after the highest peak has been refined by linear and non-linear least-squares fitting, and pre-whitened from the data. It is clear that all of the apparent 'noise' in the top panel is spectral window pattern. The bottom panel shows a least-squares fit of a sinusoid to the same data where the best-fitting frequency, $f = 0.2470 \, \text{d}^{-1}$, is clear.

Using a Discrete Fourier Transform (Kurtz 1985) and the programme PERIOD04 (Lenz & Breger 2005), we found a highest peak in the amplitude spectrum of the FORS 1 $B_z$ data (comprising 13 measurements) of $f = 0.2477 \, \text{d}^{-1}$; using least-squares fitting of a sinusoid we found $f = 0.2470 \, \text{d}^{-1}$, as is seen in Fig. 1. We refined the fitted frequency and calculated uncertainties using non-linear least-squares fitting, fitting the function:

$$B_z = A_0 + A \cos[2\pi f (t - t_0) + \phi],  \quad (1)$$

which gives our final values:

$$f = 0.246975 \pm 0.000005 \, \text{d}^{-1},$$

$$P_{\text{rot}} = 4.04899 \pm 0.00008 \, \text{d},$$

$$A_0 = -5127 \pm 34 \, \text{G},$$

$$A = 4824 \pm 40 \, \text{G},$$

$$\phi = 0.000 \pm 0.010 \, \text{rad, where}$$

$$t_0 = \text{BJD} \, 245\,4509.550 \pm 0.006,$$

$$\sigma = 121 \, \text{G}.$$

The standard deviation $\sigma$ is per measurement with respect to the fit. The error on $A_0$ is thus $\sigma/\sqrt{13}$, where $N = 13$ data points. The error on $t_0$ is the error in phase divided by $2\pi f$. We thus get an ephemeris of

$$B_z^{\text{max}} = \text{BJD} \, 245\,4509.550 \pm 0.006 + 4.04899 \pm 0.00008 E.  \quad (2)$$

The value of the rotation period is consistent with that determined by Freyhammer et al. (2008) from ASAS photometry.

## 4 THE STELLAR PARAMETERS

As an initial step to determine the fundamental stellar parameters, we employed previous photometric observations. We used the $uvby\beta$ photometry by Martinez (1993) and the UVBYBETA program written by T. T. Moon and modified by Napiwotzki, Schoenberner & Wenske (1993) based on the grid published in Moon & Dworetsky (1985). We derived an effective temperature, $T_{\text{eff}} = 9600 \, \text{K}$, and a gravity of $\log g = 4.47$ (cgs). The surface gravity is an issue, since it is known that photometric calibrations of the $c_1$ index, which are useful for determination of luminosity (hence surface gravity) for normal stars, are not entirely suitable for Ap stars, where they tend to underestimate luminosity because of heavy line blanketing in the $v$ filter. The effective temperature estimate, on the other hand, usually needs only a small correction (e.g. Hubrig, North & Mathys 2000). The reliability of the gravity estimate from Strömgren photometry is discussed by North & Kroll (1989). From Geneva photometry[1] (Mermilliod, Mermilliod & Hauck 1997) and using different calibrations (Cramer & Maeder 1979; North & Nicolet 1990; Hauck & North 1993), we obtained effective temperature estimates from 9300 to 9900 K. These, together with the estimate from $uvby\beta$, give an average photometrically determined value of $T_{\text{eff}} = 9600 \pm 300 \, \text{K}$. Interstellar reddening is negligible for this star. There is no clear evidence of any interstellar component in the Na I D1 and D2 lines, which show doublet splitting and belong to the star; any interstellar component is below 0.05 Å in equivalent width. This yields an upper limit to the colour excess of only $E(B - V) < 0.02$ (Munari & Zwitter 1997).

The Balmer lines profiles are sensitive to effective temperature and gravity. Reliable determination of the right continuum for them – especially for echelle spectra – is not an easy task and may be a source of scatter and errors. In the case of HD 75049, magnetic broadening is large and needs to be taken into account in the Balmer lines too. That small variations of Balmer lines may occur has long been known, as discussed recently by, e.g., Valyavin et al. (2007)

[1] http://obswww.unige.ch/gcpd/gcpd.html

and Elkin et al. (2008). Balmer lines profiles of H$\alpha$, H$\beta$ and H$\gamma$ in the FEROS spectrum, H$\beta$ and H$\gamma$ in the FORS 1 spectra and H$\alpha$ in the UVES spectra were compared with synthetic profiles for best fits as a function of $T_{\rm eff}$ and log $g$. An average gives $T_{\rm eff} = 9700 \pm 170$ K and log $g = 4.07 \pm 0.28$. The comparison between the observed and synthetic profiles of the Balmer lines gives acceptable agreement for a model with $T_{\rm eff} = 9600$ K and log $g = 4.0$. Synthetic calculations of the Balmer profiles were done with the SYNTH code of Piskunov (1992). Model atmospheres by Kurucz (1979) and from the Vienna New Model Grid of Stellar Atmospheres (NEMO) data base (Heiter et al. 2002) were used.

# 5 MAGNETIC FIELD

## 5.1 Longitudinal field

From observations with FORS 1, the variable mean longitudinal magnetic field $B_z$ was determined. Table 2 gives the results obtained for three methods of calculation when various lists of spectral lines and spectral regions are used. There are no differences between $B_z$ obtained from all the spectral lines in two spectral regions, 3212–6215 Å and the shorter 3705–6215 Å. But there are shifts of around 600 G between the latter and measurements from the hydrogen lines. These differences most likely reflect the uncertainties involved in the interpretation of the observed circular polarization signal in terms of a magnetic field, which arise from the statistical nature of the measurement (the considered spectral ranges include many lines of different elements, which have different magnetic sensitivities) or from the complexity of the physical foundations of the treatment of the formation of hydrogen lines in A-type star atmospheres in the presence of a magnetic field (Mathys et al. 2000). Differences in the non-uniform distribution of chemical elements in the stellar atmosphere may also contribute, but seem unlikely to represent the dominant effect. The phase curves for all the three methods are similar and show sine curves. The distribution of hydrogen in the stellar atmosphere is more homogeneous than for other chemical species. Therefore, we used results from hydrogen (last column in Table 2) for further analysis.

## 5.2 Mean magnetic field modulus

The mean magnetic field modulus $\langle B \rangle$ was determined from high-resolution spectra using the resolved Zeeman components of several spectral lines. Using Gaussian fitting, we determined the centres of the shifted Zeeman $\sigma$ components. The distance between these two components in a spectral line is proportional to the value of magnetic field modulus $\langle B \rangle$ (Mathys et al. 1997),

$$\Delta\lambda = 9.34 \times 10^{-13} g_{\rm eff} \langle B \rangle \lambda_0^2, \tag{3}$$

where wavelength is measured in Å, and $g_{\rm eff}$ is an effective Landé factor. This relation is valid in fairly general conditions for lines with the doublet or triplet Zeeman patterns; in the general case of more complex, anomalous patterns, it represents only a first approximation. Furthermore, it is based on the assumption that the Doppler effect due to stellar rotation is small compared to the magnetic splitting of the line. The latter is not strictly fulfilled in HD 75049. The resulting asymmetries of the line components, mostly seen between phases 0.85 and 0.35, further hamper the accurate determination of the field modulus.

Since the star is spotted, the actual field strength measured is somewhat dependent on the surface distribution of ions from whose lines the measurements were made. Thus, we determined the maximum field strength according to the set of spectral lines used. Table 3 presents our measurements of $\langle B \rangle$ for some spectral lines. Because of the exceptional strength of the magnetic field, the spectral line of Fe II 6149 Å, which lends itself well to the accurate determination of the mean field modulus in Ap stars and has been frequently used to this effect, is strongly distorted by the partial Paschen–Back effect, and its splitting into several components cannot be readily interpreted, so that we did not consider it. In such a strong field, the majority of spectral lines shows the resolved Zeeman splitting, but many are not strong enough for precise measurements. Many other lines are blends and cannot be used either. The most precise and reliable line splitting measurements were obtained for the strong line Fe II $\lambda$5018 Å. Their mean uncertainties can be estimated from the standard deviation of the individual measurements about a least-squares fit of the superposition of a sinusoid and of its first harmonic

**Table 3.** The magnetic field modulus $\langle B \rangle$ (kG) in HD 75049 determined from the resolved Zeeman components in some selected spectral lines. Because of the non-uniform surface abundance distributions of various ions, some of the differences in field strength at specific rotation phases may be attributable to the distribution of elements. Less reliable results are identified by question marks.

| BJD | Phase | Fe II 5018 Å | Nd III 5050 Å | Cr II 5237 Å | Nd III 6145 Å | Nd III 6327 Å | Eu II 6437 Å |
|---|---|---|---|---|---|---|---|
| 245 4141.669 63 | 0.1550 | 26.08 | 26.58 | 26.83 | 26.67 | 26.34 | 29.49 |
| 245 4171.504 22 | 0.5234 | 29.54 | 28.76 | 28.23 | 29.68 | 28.44 | 30.10 |
| 245 4387.815 93 | 0.9470 | 25.66 | 26.58 | 25.91 | 28.32 | 26.05 | 28.78 |
| 245 4432.824 89 | 0.0631 | 24.65 | 25.19? | 25.14 | 25.72 | 26.08 | 29.05 |
| 245 4451.833 66 | 0.7578 | 27.99 | 27.98 | 27.68 | 29.12 | 28.01 | 29.62 |
| 245 4455.702 26 | 0.7133 | 28.46 | 28.29 | 27.91 | 29.12 | 28.38 | 29.87 |
| 245 4468.845 89 | 0.9594 | 25.24 | 25.82 | 25.64 | 28.10 | 26.08 | 28.67 |
| 245 4481.814 65 | 0.1624 | 26.83 | 26.64 | 27.97 | 27.13 | 28.73 | 29.64 |
| 245 4513.788 92 | 0.0593 | 24.25 | 24.74? | 24.84? | 23.27? | | |
| 245 4516.689 04 | 0.7755 | 27.73 | 27.69 | 27.48 | 29.20 | 27.60 | 29.52 |
| 245 4524.664 61 | 0.7453 | 28.04 | 27.98 | 27.83 | 29.26 | 28.21 | 29.62 |
| 245 4544.516 08 | 0.6481 | 28.96 | 28.60 | 28.18 | 29.40 | 28.38 | 30.06 |
| 245 4547.511 27 | 0.3878 | 29.51 | 28.44 | 28.57 | 29.63 | 29.10 | 30.04 |
| 245 4557.590 95 | 0.8773 | 26.45 | 26.49 | 26.71 | 28.77 | 26.77 | 29.98 |

against rotation phase. They are found in this way to be of the order of 0.27 kG.

### 5.3 Dipole model

From Harmanec (1988), we estimate for a main-sequence A star with $T_{eff} = 9600$ K that the stellar radius will be around 2.1 $R_{\odot}$. This value agrees well with other published estimations of stellar radii. While main-sequence stars with a similar temperature may range in radius between 1.7 and 5 $R_{\odot}$ from the zero-age main sequence to the terminal-age main sequence, a radius more than 2.4 $R_{\odot}$ is ruled out for HD 75049, as it requires an implausibly high polar magnetic field in comparison with the observed magnetic field modulus for the dipole model discussed in the next section. The range of possible radius for HD 75049 is therefore between 1.7 and 2.4 $R_{\odot}$.

The spectral lines with zero Landé factor, and the resolved Zeeman components of lines with large Landé factors, give $v \sin i = 8.5 \pm 1.0$ km s$^{-1}$. From the relation $v_{eq} = (50.59R)/P$, where $P$ is measured in days, we derive a rotational inclination of $i = 23°6 \pm 3°0$ and an equatorial velocity $v_{eq} = 21.2$ km s$^{-1}$ for 1.7 $R_{\odot}$, and $i = 16°5 \pm 2°0$ and $v_{eq} = 30.0$ km s$^{-1}$ for 2.4 $R_{\odot}$.

From least-squares fitting with the PERIOD04 program (Lenz & Breger 2005), for the hydrogen lines we have an average $B_z = -5.76$ kG which varies with an amplitude of $4.89 \pm 0.06$ kG. From expressions for an oblique rotator (e.g. Preston 1967), we find a magnetic obliquity in the range $\beta = 63° \pm 3°0$ for star with radius 1.7 $R_{\odot}$ to $\beta = 71° \pm 3°0$ for 2.4 $R_{\odot}$. Following the approach of Stibbs (1950) and Preston (1970), we calculated a grid of models using the above parameter range and found a best fit for $B_p = 42 \pm 2$ kG, $i = 25° \pm 3°$ and $\beta = 60° \pm 3°$, values that are suitable for a stellar radius of 1.7 $R_{\odot}$. The variation of the longitudinal magnetic field $B_z$ with the rotational period and selected model fitting is shown in the top panel of Fig. 2. We can get an equally good fit to the top panel of Fig. 2 with the parameters $R = 2.4 R_{\odot}$, $i = 16°5$, $\beta = 71°$ and $B_p = 60$ kG, but then the model curve for $\langle B \rangle$ in the bottom panel has a minimum of 38 kG, which is clearly wrong. Under the assumption that the field geometry is dipolar, the implication of this is that HD 75049 is close to the zero-age main sequence.

Variations of $\langle B \rangle$ show less symmetric curves than that for $B_z$. To fit the $\langle B \rangle$ curve for Fe II 5018 Å, we had to employ a sine curve with its first harmonic. Our centred dipole model does not fit the variation of this Fe II line but is acceptable for lines of Nd III and Eu II, considering the errors of measurement and non-uniform distribution of chemical elements. Otherwise the magnetic field geometry is more complicated than a simple dipole, as is typical for many magnetic Ap stars (e.g. Landstreet & Mathys 2000).

### 5.4 Correlation between magnetic and spectral variability

One sees in Fig. 2 that the field modulus measurements obtained from the three sets of analysed lines show different amplitudes of variation. The Fe-based measurements vary with the largest amplitude, while the lowest variation amplitude is observed for $\langle B \rangle$ values derived from consideration of the Eu lines. These differences may find their origin in part in differences in the non-uniform distribution of the various elements of interest over the stellar surface. In order to test this interpretation, we have checked the dependence on rotation phase of the equivalent widths and radial velocities of lines of the considered elements. The examples in Fig. 3 illustrate the observed behaviours. The spectral lines that are shown, Cr II λ5334 Å, Fe II λ5432 Å and Nd III λ6145 Å, are representative of all
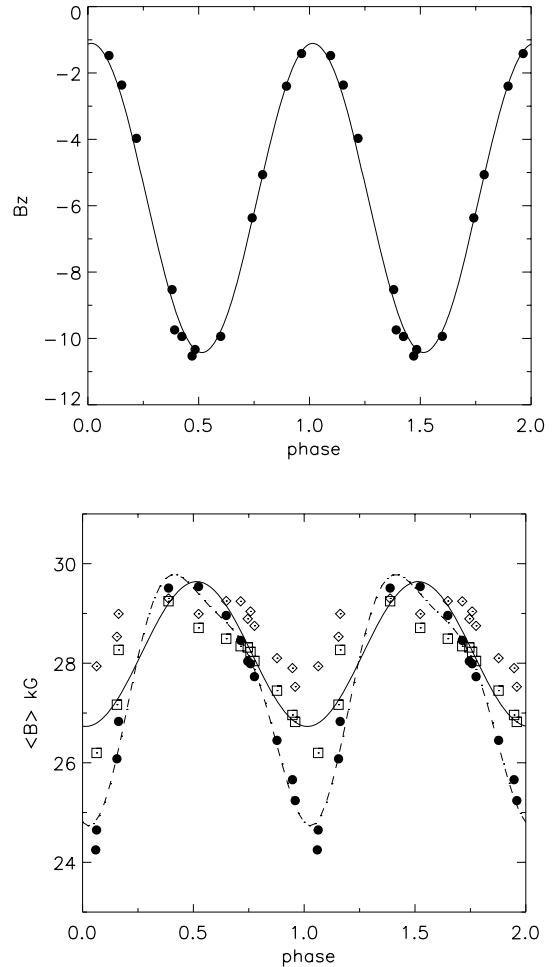


**Figure 2.** Top panel: the variation of the longitudinal magnetic field $B_z$ with rotational period for HD 75049. Filled circles are observations with FORS 1 using the hydrogen lines. The curve is a centred dipole model for $B_p = 42$ kG, $i = 25°$ and $\beta = 60°$. Bottom panel: the variation of the magnetic field modulus $\langle B \rangle$ with rotational period for HD 75049 from our UVES and FEROS data. Different symbols are used to represent measurements performed using lines of different ions: filled circles for Fe II λλ5018 Å, open squares for Nd III using four lines at λλ5050, 5845, 6145 and 6327 Å, and diamonds for Eu II using two lines at λλ6049 and 6437 Å. The solid line is the same model as for upper panel. The dashed curve is a least-squares fit of a sinusoid plus first harmonic to the Fe II data.

the reasonably unblended lines of the elements from which they arise. Equivalent width variations are definitely observed for Cr and Nd, but they are not definitely detected for Fe. The Nd lines also show radial velocity variations, while our data show no clear indications of such variations for Cr and Fe. Even after averaging the radial velocity measurements of several lines of these elements, no convincing evidence for variability was found.

For Nd, maximum equivalent width occurs close to phase 0.5, hence to the negative extremum of the longitudinal field and to the maximum of the field modulus. The radial velocities of the Nd lines vary in phase quadrature with their equivalent widths; the lines are blueshifted between phases 0 and 0.5, and redshifted between phases 0.5 and 1.0. This is consistent with the presence of a region of enhanced abundance ('spot') of Nd around the negative magnetic pole. The same conclusion applies to Eu, whose lines show similar variability to those of Nd.
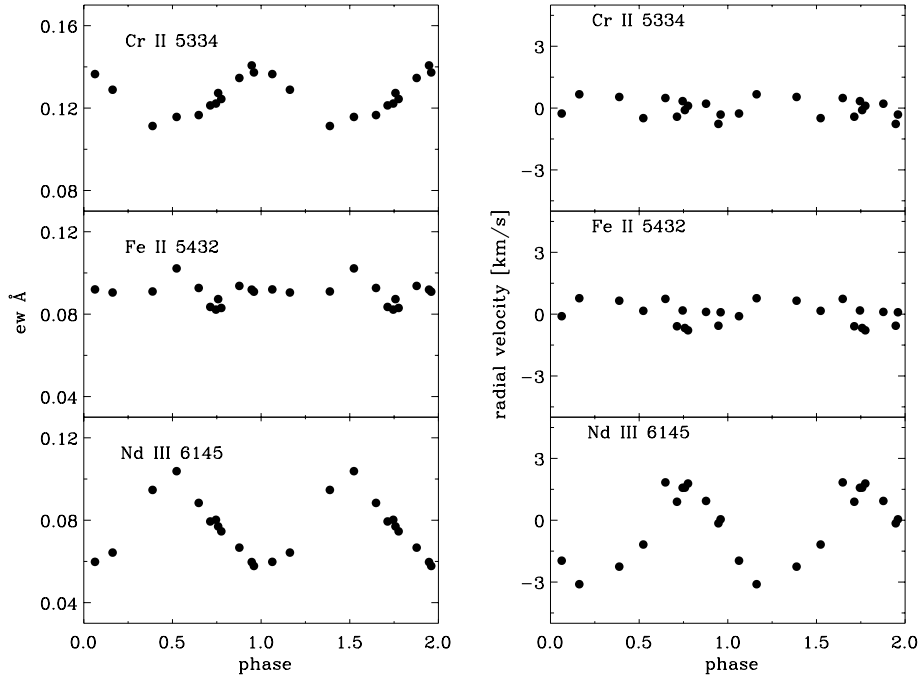
**Figure 3.** Variation with rotation phase of the equivalent width (left) and the radial velocity (right) of the lines Cr II λ5334 Å, Fe II λ5432 Å and Nd III λ6145 Å.

The equivalent widths of the Cr lines show the opposite variation, reaching their minimum close to phase 0.5 and being largest close to phase 0. Any radial velocity variations that they may show do not clearly stand out of the measurement noise, so that their amplitude is definitely much lower (by a factor of 5 or more) than for Nd lines. Yet, this may not be inconsistent with equivalent width variations being due to a non-uniform distribution of Cr over the stellar surface such that the abundance of this element is minimum around the negative pole and increases away from it. Possible configurations include a band of enhanced Cr abundance along the magnetic equator. With a distribution of this type, one can simultaneously observe on the visible stellar hemisphere approaching and receding Cr-rich regions, whose contributions to the radial velocity of Cr spectral lines mostly averages out in disc-integrated observations.

Finally, Fe lines do not show any definite variability of their equivalent widths or radial velocities, indicating that any abundance inhomogeneity in the distribution of this element on the visible part of the star must be moderate at most. Si behaves like Fe.

Thus, we are left with the qualitative picture of a star showing a concentration of Nd and Eu and a (relative) depletion of Cr around its negative magnetic pole, with a comparatively uniform distribution of Fe and Si over its surface. One should keep in mind, though, that due to the low inclination of the rotation axis on the line of sight, a large fraction of the stellar surface is never observed.

The non-uniform distribution of Nd over the stellar surface may account for part of the differences between the values of ⟨B⟩ that are derived from measurements of its lines and from those of Fe, whose abundance appears much more constant across the star. However, it is unlikely to be the only factor, or even the main one. If it were, one would, for instance, expect greater values of the field modulus to be determined from Nd lines than from Fe lines close to phase 0.5; the opposite is observed in Fig. 2. Most likely, the origin of the difference should be sought elsewhere. In particular, one should bear in mind that Nd lines are subject to hyperfine structure. This introduces severe complications in the treatment of their formation in

the presence of a strong magnetic field, as illustrated, e.g., in Landi Degl'Innocenti (1975). Accordingly, the physical meaning of the value of ⟨B⟩ that is obtained by the application of equation (3) to the observed splitting of Nd lines is not fully clear. In particular, one cannot a priori expect it to provide a measurement of the mean magnetic field modulus that is consistent with its determinations from analysis of Fe lines, which rests on a firmer physical basis. The same applies to the usage of Eu lines to measure ⟨B⟩. The differences seen in Fig. 2 between the variation curves of this field moment resulting from measurements of the Nd III and Eu II lines would actually be very difficult to understand in terms of abundance inhomogeneities since the equivalent width and radial velocity behaviours indicate that, to first order, the distribution of both elements over the stellar surface is similar. On the other hand, around phase 0, the lines Eu II λλ6049, 6437 Å become very weak and shallow, so that the uncertainties of the ⟨B⟩ determinations based on them become very large, and the values obtained for this field moment between phases ∼0.9 and ∼0.2 should be considered with appropriate caution.

## 6 ASYMMETRY OF SPECTRAL LINES

Spectral lines in HD 75049 show significant variability with rotation period, and for many lines we also note asymmetry in the Zeeman patterns, as can be seen in Fig. 4. Shifted σ components normally are symmetric with respect to the line centre, according to the classical Zeeman theory. Observations of magnetic Ap stars reveal more complicated behaviours of the Zeeman patterns. Spectral line asymmetry is often visible in high-resolution spectra of Ap stars. While non-uniform distribution of chemical species on the stellar surface contributes to this, the main source of line asymmetry more often is the variable combination of the Zeeman and Doppler effects across the stellar surface. Indeed, due to the large-scale structure of the magnetic field, the Zeeman and Doppler shifts are correlated across the stellar disc, and this correlation is reflected in the shapes of the disc-integrated spectral lines.
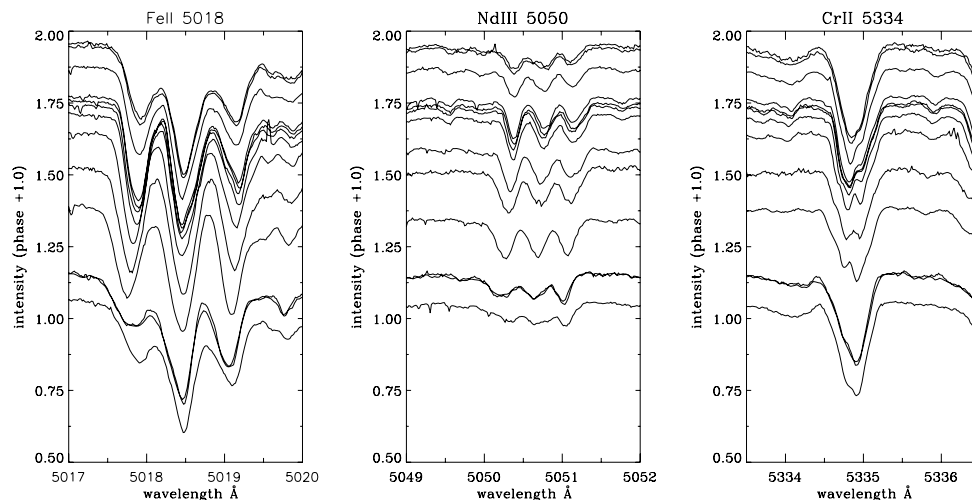
**Figure 4.** Variation with rotation phase of the observed profiles of the spectral lines Fe II λ5018 Å , Nd III λ5050 Å and Cr II λ5334 Å. Each spectrum is shifted vertically from the normalized continuum to a value corresponding to (1 + rotation phase), hence the ordinate shows both the continuum and rotation phase.

The observed presence of this effect in HD 75049 is particularly plausible, considering that this star has a very strong magnetic field and a large $v \sin i$ for a star with magnetically resolved lines. That it is the dominant effect for explanation of the origin of the line asymmetries can be inferred from consideration of Fig. 4. Representative lines of each of the three elements Fe, Cr and Nd are seen to show qualitatively similar asymmetries: a red $\sigma$ component (or red wing) shallower and broader than its blue counterpart at phases comprised between ∼0.6 and ∼0.9, and vice-versa in the phase range ∼0.1–0.4. Since the distributions of Fe, Cr and Nd over the star differ considerably from each other, the similarity of the line asymmetries for all of them cannot arise primarily from their inhomogeneities. Also, because the magnetic field of HD 75049 is very strong, the partial Paschen–Back effect may contribute to asymmetries of a significant number of lines (Mathys 1990), but it affects different transitions to a variable extent and in qualitatively different ways, so that it cannot account for the consistent behaviours illustrated in Fig. 4.

## 7 CHEMICAL ABUNDANCES

Large overabundances of some chemical elements, especially of rare earth elements, is one of the defining characteristics of Ap stars. Various chemical elements concentrate in different places on the surface of the star. There is a tendency for rare earth elements to concentrate around the magnetic poles in some sort of spots. The size and number of spots may vary (Kochukhov et al. 2004; Freyhammer et al. 2009). The situation is even more complex since the atmospheres of Ap stars also show vertical stratification (e.g. Babel & Lanz 1992; Wade et al. 2001; Kochukhov, Shulyak & Ryabchikova 2009) where various elements accumulate in different layers in the atmosphere.

Because of the spotted structure of Ap stars, average abundances do not reflect the complexity of the physical conditions at the stellar surface, yet they are useful for statistical analysis and comparison of stars in the class (e.g. Adelman 1973; Ryabchikova et al. 2004). HD 75049 has a rich spectrum, but is not extraordinarily peculiar. In the spectrum, many lines of rare earth elements are visible, but the majority of the strongest metal lines belongs to Si II, Ti II, Fe II and Cr II. Lines of Sr II in the blue region of the FEROS spectrum are also rather strong.
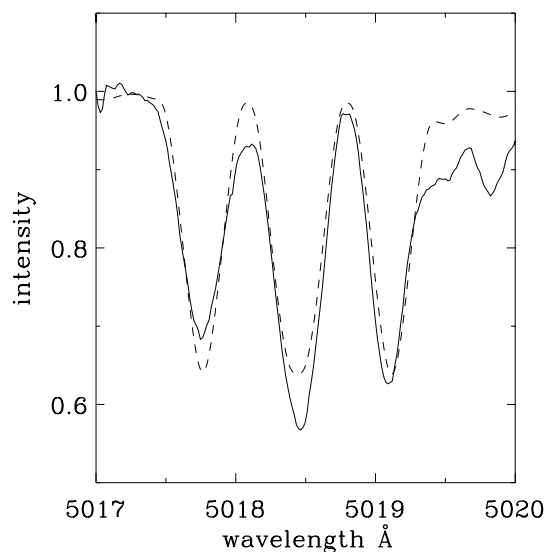


**Figure 5.** Observed (solid line) and synthetic (dashed line) profiles for Fe II 5018 Å.

We obtained the abundances of several elements using spectral synthesis where the observed spectra were compared with synthetic spectra until a best fit was obtained. An example for Fe II λ5018 Å is shown in Fig. 5. The synthetic spectra were calculated with the software SYNTHMAG (Piskunov 1999). The spectral line list was taken from the Vienna Atomic Line Data base (Kupka et al. 1999), which includes lines of rare earth elements from the Database on Rare Earths At Mons University (DREAM) (Biémont, Palmeri & Quinet 1999). A model atmosphere with $T_{\mathrm{eff}} = 9600\,\mathrm{K}$ and $\log g = 4.0$ with metallicity of 0.5 dex above solar from the NEMO data base (Heiter et al. 2002) was used. The synthetic spectra provided a good match to many spectral lines with the field strength chosen, but some lines need further broadening to match the wings. Macro-turbulence is possibly not the explanation for this, as magnetic fields suppress macroscopic motion in the stellar atmospheres. With the non-uniform distribution of abundances – both horizontally and vertically – in Ap star atmospheres, it may be that stronger magnetic field strengths in different line-forming regions could explain this extra broadening. Further study is needed to test this idea.

**Table 4.** Chemical abundances for HD 75049 for selected elements and their corresponding solar abundances (Asplund et al. 2005). The errors quoted are internal standard deviations for the set of lines measured. Only an upper limit could be placed on the abundance of Nd II. Columns 3 and 5 give the number of lines used, $N_{lines}$, in each case.

| Ion | $\log N/N_{tot}$ $\phi = 0.388$ | $N_{lines}$ | $\log N/N_{tot}$ $\phi = 0.063$ | $N_{lines}$ | $\log N/N_{tot}$ Sun |
|---|---|---|---|---|---|
| Si II | $-3.70 \pm 0.05$ | 2 | $-3.55 \pm 0.05$ | 2 | $-4.49$ |
| Ti II | $-6.04 \pm 0.10$ | 2 | $-5.85 \pm 0.15$ | 2 | $-7.10$ |
| Cr II | $-4.73 \pm 0.15$ | 14 | $-4.53 \pm 0.13$ | 9 | $-6.36$ |
| Fe I | $-3.93 \pm 0.17$ | 10 | $-4.10 \pm 0.29$ | 4 | $-4.55$ |
| Fe II | $-3.89 \pm 0.15$ | 17 | $-3.98 \pm 0.15$ | 6 | $-4.55$ |
| La II | $-7.15 \pm 0.21$ | 16 | $-7.23 \pm 0.18$ | 6 | $-10.87$ |
| Ce II | $-7.48 \pm 0.16$ | 5 | $-7.95 \pm 0.05$ | 4 | $-10.42$ |
| Pr III | $-8.07 \pm 0.15$ | 4 | $-8.10 \pm 0.16$ | 4 | $-11.29$ |
| Nd III | $-7.27 \pm 0.05$ | 3 | $-7.57 \pm 0.12$ | 3 | $-10.55$ |
| Nd II | $< -8.40$ | 3 | $< -7.98$ | 3 | $-10.55$ |
| Eu II | $-7.71 \pm 0.19$ | 4 | $-8.10 \pm 0.29$ | 4 | $-11.48$ |

Two spectra at rotation phases near minimum and maximum longitudinal field strength (phase 0.063 and 0.388; see Fig. 2) were used for abundances determination. Magnetic field strengths of 26 and 30 kG, respectively, were used for calculation of the synthetic spectra at these two rotational phases. Synthetic line profiles for various abundances were compared with observed profiles for best fits. Many calculated line profiles do not fit the observed profiles perfectly as a result of blending and asymmetry, but the average value for a number of lines gives reliable results. It was more difficult to fit the spectrum observed at rotational phase 0.063 when the field strength is lower and some lines are not sharp and more asymmetric. Table 4 presents the values of the abundances with errors determined for various ions. The errors given are the internal standard deviations for the list of examined lines for each ion. There were no lines of Nd II found in the spectra, so only an upper limit is given in Table 4. The last column in the table gives solar abundances for the same elements taken from Asplund, Grevesse & Sauval (2005). HD 75049 shows overabundances of silicon, chromium and europium and thus can be considered to belong to the Si–Cr group of Ap stars, according to the classification of peculiar stars.

## 8 CONCLUDING REMARKS

The strong magnetic field of HD 75049 is an exciting discovery. This star is a rival for the long-known strongest Ap magnetic field in Babcock's star, HD 215441. Both stars have deep silicon lines, but are at opposite ends of the temperatures range of the Ap Si stellar group. Babcock (1960) noted that HD 215441 does not have outstanding peculiarities in the spectrum. We have found the same in HD 75049, which has a rich peculiar spectrum, but with overabundances of number chemical elements similar to other Ap stars with much smaller field strengths.

HD 215441 has a magnetic field modulus that changes from 32 to 35 kG over the rotational period (Babcock 1960; Preston 1969). Preston (1969) suggested that the magnetic field of this star deviates from a centred dipole. Magnetic configurations with a combination of dipole and quadrupole components (Borra & Landstreet 1978) or dipole, quadrupole and octupole (Landstreet & Mathys 2000) components were required to model both observations of $B_z$ obtained by Borra & Landstreet (1978) and $\langle B \rangle$ by Preston (1969).

In contrast, for HD 75049 the centred dipole model is a suitable first approximation to fit both the longitudinal field and field mod-

ulus measurements. Some discrepancy with the second magnetic moment dipole model may be a result of non-uniform distribution of chemical elements at surface. More complex magnetic geometry may also be present in this star. An important result is that the star is probably young. Its estimated stellar radius places it close to the zero-age main sequence.

Landstreet & Mathys (2000) examined the inclination of rotation axis $i$ to line of sight and obliquity $\beta$ of the magnetic axis to the rotation axis for a sample of magnetic Ap stars. They found that the majority of the slow rotators with periods longer than 25 d have $\beta$ smaller than 20°, while stars with short rotation periods tend to show a large obliquity of the magnetic axis. Our estimation of $\beta = 60° \pm 3°$ for HD 75049 is consistent with this conclusion.

## REFERENCES

Abt H. A., 2009, AJ, 138, 28
Adelman S. J., 1973, ApJ, 183, 95
Asplund M., Grevesse N., Sauval A. J., 2005, in Barnes T. G., III, Bash F. N., eds, ASP Conf. Ser. Vol. 336, Cosmic Abundances as Records of Stellar Evolution and Nucleosynthesis. Astron. Soc. Pac., San Francisco, p. 25
Babcock H. W., 1947, ApJ, 105, 105
Babcock H. W., 1958, ApJS, 3, 141
Babcock H. W., 1960, ApJ, 132, 521
Babel J., Lanz T., 1992, A&A, 263, 232
Biémont E., Palmeri P., Quinet P., 1999, Ap&SS, 269, 635
Borra E. F., Landstreet J. D., 1978, ApJ, 222, 226
Cramer N., Maeder A., 1979, A&A, 78, 305
Elkin V. G., Kurtz D. W., Freyhammer L. M., Hubrig S., Mathys G., 2008, MNRAS, 390, 1250
Freyhammer L. M., Elkin V. G., Kurtz D. W., Mathys G., Martinez P., 2008, MNRAS, 389, 441
Freyhammer L. M., Kurtz D. W., Elkin V. G., Mathys G., Savanov I., Zima W., Shibahashi H., Sekiguchi K., 2009, MNRAS, 396, 325
Harmanec P., 1988, Bull. Astron. Inst. Czech., 39, 329
Hauck B., North P., 1993, A&A, 269, 403
Heiter U. et al., 2002, A&A, 392, 619
Hubrig S., North P., Mathys G., 2000, ApJ, 539, 352
Hubrig S. et al., 2005, A&A, 440, L37
Hubrig S., North P., Schöller M., Mathys G., 2006, Astron. Nachr., 327, 289
Hubrig S., Mathys G., Kurtz D. W., Schöller M., Elkin V. G., Henrichs H. F., 2009, MNRAS, 657
Kochukhov O., 2006, A&A, 454, 321
Kochukhov O., Drake N. A., Piskunov N., de la Reza R., 2004, A&A, 424, 935
Kochukhov O., Shulyak D., Ryabchikova T., 2009, A&A, 499, 851
Kudryavtsev D. O., Romanyuk I. I., Elkin V. G., Paunzen E., 2006, MNRAS, 372, 1804
Kupka F., Piskunov N., Ryabchikova T. A., Stempels H. C., Weiss W. W., 1999, A&AS, 138, 119
Kurtz D. W., 1985, MNRAS, 213, 773
Kurtz D. W., Elkin V. G., Cunha M. S., Mathys G., Hubrig S., Wolff B., Savanov I., 2006, MNRAS, 372, 286
Kurucz R. L., 1979, ApJS, 40, 1

Landi Degl'Innocenti E., 1975, A&A, 45, 269

Landstreet J. D., Mathys G., 2000, A&A, 359, 213

Lenz P., Breger M., 2005, Commun. Asteroseismol., 146, 53

Martinez P., 1993, PhD Thesis, Univ. Cape Town

Mathys G., 1990, A&A, 232, 151

Mathys G., 1991, A&AS, 89, 121

Mathys G., 1995, A&A, 293, 746

Mathys G., Hubrig S., Landstreet J. D., Lanz T., Manfroid J., 1997, A&AS, 123, 353

Mathys G., Stehlé C., Brillant S., Lanz T., 2000, A&A, 358, 1151

Mermilliod J.-C., Mermilliod M., Hauck B., 1997, A&AS, 124, 349

Moon T. T., Dworetsky M. M., 1985, MNRAS, 217, 305

Munari U., Zwitter T., 1997, A&A, 318, 269

Napiwotzki R., Schoenberner D., Wenske V., 1993, A&A, 268, 653

North P., Kroll R., 1989, A&AS, 78, 325

North P., Nicolet B., 1990, A&A, 228, 78

Pojmanski G., 2002, Acta Astron., 52, 397

Piskunov N. E., 1992, in Glagolevskij Yu. V., Romanyuk I. I., eds, Stellar Magnetism. Nauka, St Petersburg, p. 92

Piskunov N., 1999, in Nagendra K. N., Stenflo J. O., eds, Astrophys. Space Sci. Library Vol. 243, Solar Polarization. Kluwer, Dordrecht, p. 515

Preston G. W., 1967, ApJ, 150, 547

Preston G. W., 1969, ApJ, 156, 967

Preston G. W., 1970, ApJ, 160, 1059

Ryabchikova T., Nesvacil N., Weiss W. W., Kochukhov O., Stütz C., 2004, A&A, 423, 705

Stibbs D. W. N., 1950, MNRAS, 110, 395

Valyavin G., Lee B.-C., Shulyak D., Han I., Kochukhov O., Khang D.-I., Kim K.-M., 2007, in Kang Y. W., Lee H. W., Leung K. C., Cheng K. S., eds, ASP Conf. Ser. Vol. 362, The Seventh Pacific Rim Conference on Stellar Astrophysics. Astron. Soc. Pac., San Francisco, p. 245

Wade G. A., Ryabchikova T. A., Bagnulo S., Piskunov N., 2001, in Mathys G., Solanki S. K., Wickramasinghe D. T., eds, ASP Conf. Ser. Vol. 248, Magnetic Fields Across the Hertzsprung–Russell Diagram. Astron. Soc. Pac., San Francisco, p. 373

This paper has been typeset from a TEX/LATEX file prepared by the author.